Rapid whole-brain quantitative MT imaging

Afshari, Roya ; Santini, Francesco ; Heule, Rahel ; Meyer, Craig H ; Pfeuffer, Josef ; Bieri, Oliver

Abstract: PURPOSE To provide a robust whole-brain quantitative magnetization transfer (MT) imaging method that is not limited by long acquisition times. METHODS Two variants of a spiral 2D interleaved multi-slice spoiled gradient echo (SPGR) sequence are used for rapid quantitative MT imaging of the brain at 3 T. A dual flip angle, steady-state prepared, double-contrast method is used for combined B_1 and-T_1 mapping in combination with a single-contrast MT-prepared acquisition over a range of different saturation flip angles (50 deg to 850 deg) and offset frequencies (1 kHz and 10 kHz). Five sets (containing minimum 6 to maximum 18 scans) with different MT-weightings were acquired. In addition, main magnetic field inhomogeneities (ΔB_0) were measured from two Cartesian low-resolution 2D SPGR scans with different echo times. Quantitative MT model parameters were derived from all sets using a two-pool continuous-wave model analysis, yielding the pool-size ratio, F, their exchange rate, k_f, and their transverse relaxation time, T_{2r}. RESULTS Whole-brain quantitative MT imaging was feasible for all sets with total acquisition times ranging from 7:15 min down to 3:15 min. For accurate modeling, B_1-correction was essential for all investigated sets, whereas ΔB_0-correction showed limited bias for the observed maximum off-resonances at 3 T. CONCLUSION The combination of rapid B_1-T_1 mapping and MT-weighted imaging using a 2D multi-slice spiral SPGR research sequence offers excellent prospects for rapid whole-brain quantitative MT imaging in the clinical setting.

DOI: https://doi.org/10.1016/j.zemedi.2023.02.005

ORIGINAL PAPER

Rapid whole-brain quantitative MT imaging

Roya Afshari [a,b,*], **Francesco Santini** [a,c], **Rahel Heule** [d,e], **Craig H. Meyer** [f], **Josef Pfeuffer** [g], **Oliver Bieri** [a,b]

[a] Division of Radiological Physics, Department of Radiology, University Hospital Basel, Basel, Switzerland
[b] Department of Biomedical Engineering, University of Basel, Basel, Switzerland
[c] BAMM group, Department of Biomedical Engineering, University of Basel, Basel, Switzerland
[d] High Field Magnetic Resonance, Max Planck Institute for Biological Cybernetics, Tübingen, Germany
[e] Department of Biomedical Magnetic Resonance, University of Tübingen, Tübingen, Germany
[f] Department of Biomedical Engineering, University of Virginia, Charlottesville, VA, USA
[g] Siemens Healthcare, Application Development, Erlangen, Germany

Received 24 November 2022; accepted 11 February 2023

Abstract

Purpose: To provide a robust whole-brain quantitative magnetization transfer (MT) imaging method that is not limited by long acquisition times.
Methods: Two variants of a spiral 2D interleaved multi-slice spoiled gradient echo (SPGR) sequence are used for rapid quantitative MT imaging of the brain at 3 T. A dual flip angle, steady-state prepared, double-contrast method is used for combined B_1 and-T_1 mapping in combination with a single-contrast MT-prepared acquisition over a range of different saturation flip angles (50 deg to 850 deg) and offset frequencies (1 kHz and 10 kHz). Five sets (containing minimum 6 to maximum 18 scans) with different MT-weightings were acquired. In addition, main magnetic field inhomogeneities (ΔB_0) were measured from two Cartesian low-resolution 2D SPGR scans with different echo times. Quantitative MT model parameters were derived from all sets using a two-pool continuous-wave model analysis, yielding the pool-size ratio, F, their exchange rate, k_f, and their transverse relaxation time, T_{2r}.
Results: Whole-brain quantitative MT imaging was feasible for all sets with total acquisition times ranging from 7:15 min down to 3:15 min. For accurate modeling, B_1-correction was essential for all investigated sets, whereas ΔB_0-correction showed limited bias for the observed maximum off-resonances at 3 T.
Conclusion: The combination of rapid B_1-T_1 mapping and MT-weighted imaging using a 2D multi-slice spiral SPGR research sequence offers excellent prospects for rapid whole-brain quantitative MT imaging in the clinical setting.

Keywords: Magnetization transfer; qMT; Spiral; B_1; Correction; Brain

Introduction

In its simplest and traditional form, magnetization transfer (MT) contrast [1] is quantified from the acquisition of two scans: one without and one with the MT-preparation module [2]. The two signals are then condensed within the so-called magnetization transfer ratio (MTR) and a great effort has been undertaken to ensure high reproducibility taking into account intrinsic, as well as possible extrinsic, confounding factors [3]. It has, however, also been realized

* Corresponding author: Roya Afshari, Division of Radiological Physics, Department of Radiology, University Hospital Basel, Petersgraben 4, 4051 Basel, Switzerland.
E-mail: roya.afshari@unibas.ch (R. Afshari).

Z Med Phys **xxx** (2023) xxx–xxx
https://doi.org/10.1016/j.zemedi.2023.02.005
www.elsevier.com/locate/zemedi

that the phenomenological reduction of a complex tissue system down to a single parameter may lack pathologic specificity making MTR results incomplete and controversial, especially in the brain [4]. As a result, biophysical models of MT have been developed that allow the quantitative estimation of the compartmental tissue properties. To this end, two-compartment (or binary) spin-bath models are most commonly considered to yield quantitative MT parameter (qMT) estimates, such as the pool-size ratio of the two compartments, their rate of magnetization exchange, and the compartmental relaxation properties [5-8]. As with any other quantitative MRI method, however, accurate estimation of the underlying tissue model parameters may depend on deviations from the presumed radiofrequency (RF) excitation field (B_1), and inhomogeneities in the main magnetic field (ΔB_0).

Generally, qMT imaging requires multiple MT-weighted measurements and thus prolonged image acquisitions which may prevent widespread clinical use and applicability [6,8]. This can, for instance, be addressed by a reduction of the number of free MT model parameters (thus reducing the number of measurements) [8,9].Alternatively, rapid imaging concepts, such as MT-sensitized balanced steady state free precession (bSSFP) [10] or highly efficient k-space sampling schemes, such as MT-sensitized single-shot echo planar imaging (EPI) [11] can be used to reduce the scan time for qMT imaging down to ~10-15 min.

Only recently, a spiral imaging concept was proposed for rapid whole-brain MTR imaging with intrinsic B_1-correction within less than one minute [12]. The method takes advantage of an MT-weighted multi-slice spiral spoiled gradient echo (SPGR) research sequence offering whole-brain coverage for the acquisition of a single MT-weighted volume within 20 s. Notably, the same underlying spiral SPGR research sequence was also suggested for rapid intrinsically B_1-corrected whole-brain T_1 mapping in less than one minute [13–15]. In this work, we thus propose to fuse these two concepts for rapid, whole-brain, in-vivo qMT imaging using a two-pool model analysis. We will show that the proposed method allows rapid whole-brain qMT imaging in less than typically 5 minutes thus being compatible with the clinical workflow.

Methods

Imaging sequences and image reconstruction

MT-weighted imaging was performed with an interleaved, multi-slice, spiral SPGR research sequence, as described in [12,13]. The MT-preparation module had a duration of 19.1 ms and consisted of a 17.92 ms non-selective, unapodized, Gaussian-shaped, radio-frequency saturation pulse with variable frequency offset (Δ) and variable flip angle (β) and crusher gradients. Slice selection was performed with a sinc-shaped RF pulse of 0.6 ms duration and a time-bandwidth-product of 1.6. A flip angle of $\alpha = 25$ deg and a slice thickness of 3 mm was used. The total acquisition duration of the imaging kernel (including slice selection, spiral readout, and crusher gradients) was 9.75 ms.

For each slice, $N_{sp} = 20$ spiral interleaves in combination with an acceleration factor of two were used; thus effectively reducing the acquisition to 10 spiral readouts per slice. Data was reconstructed online on the scanner with an in-plane resolution of 1.3×1.3 mm^2 using a spiral version of the "iTerative Self-consistent Parallel Imaging Reconstruction" method (SPIRiT) [16]. An auto-stop criterion was used, also when the k-space was fully sampled at the Nyquist rate, to implicitly derive the optimal density compensation function for the gridding algorithm. A single high-resolution MT-weighted volume was reconstructed from the acquisition of $N_{sl} = 50$ interleaved slices with a repetition time (TR) of 1650 ms (Fig. 1). The overall acquisition time for a single MT-weighted whole-brain volume was 19.8 s; including a dummy preparation period of 2×TR (i.e., without readout) to reach the steady state for tissues (see Fig. 1A).

In addition, a T_1-map and a low-resolution B_1-map were acquired based on the same spiral research sequence, described in detail in [13]. Generally, B_1 field inhomogeneities lead to local deviations from the nominal flip angle, $\alpha_{nom} \rightarrow \alpha_{act} = \zeta_{B1} \cdot \alpha_{nom}$, using a scaling factor ζ_{B1}. Essentially, the same resolution and number of slices were used as for the MT-weighted scans [17]. Two scans with optimal variable flip angles (VFA) of 17 deg and 80 deg for a TR of 250 ms were used. The overall acquisition time for the combined B_1 ($\equiv \zeta_{B1}$) and-T_1 mapping was 53 s.

Moreover, a ΔB_0 map (as usual given in Hz via the association $\Delta B_0 \mapsto \gamma \cdot \Delta B_0$) was derived from the acquisition of two multi-slice GRE volumes with different echo times, $TE_1 = 1.45$ ms and $TE_2 = 1.90$ ms. Each acquisition had 50 slices with slice thickness of 3 mm measured with a TR of 180 ms, in-plane resolution of 1.3×1.3 mm^2, and FOV of 256×256 mm^2. The total acquisition time for the ΔB_0 mapping was 22 s.

MT signal modeling and numerical simulation

From the interleaved slice acquisition (see Fig. 1B), pulsed MT-contrast in each slice is generated by a train of N_{sl} MT pulses separated by short free precession periods (see Fig. 1C), having an effective duration of 1650 ms (TR) and corresponding mean saturation rate $\bar{W}$ [18]:

$$\bar{W} = N_{sl}\frac{\pi}{TR}\int_0^{T_{RF}} \omega_1^2(t)dtG(\Delta) \quad (1)$$

where $G(\Delta)$ is the absorption line shape, which is assumed to be super-Lorentzian for tissues, and $\bar{W}$ depends on the

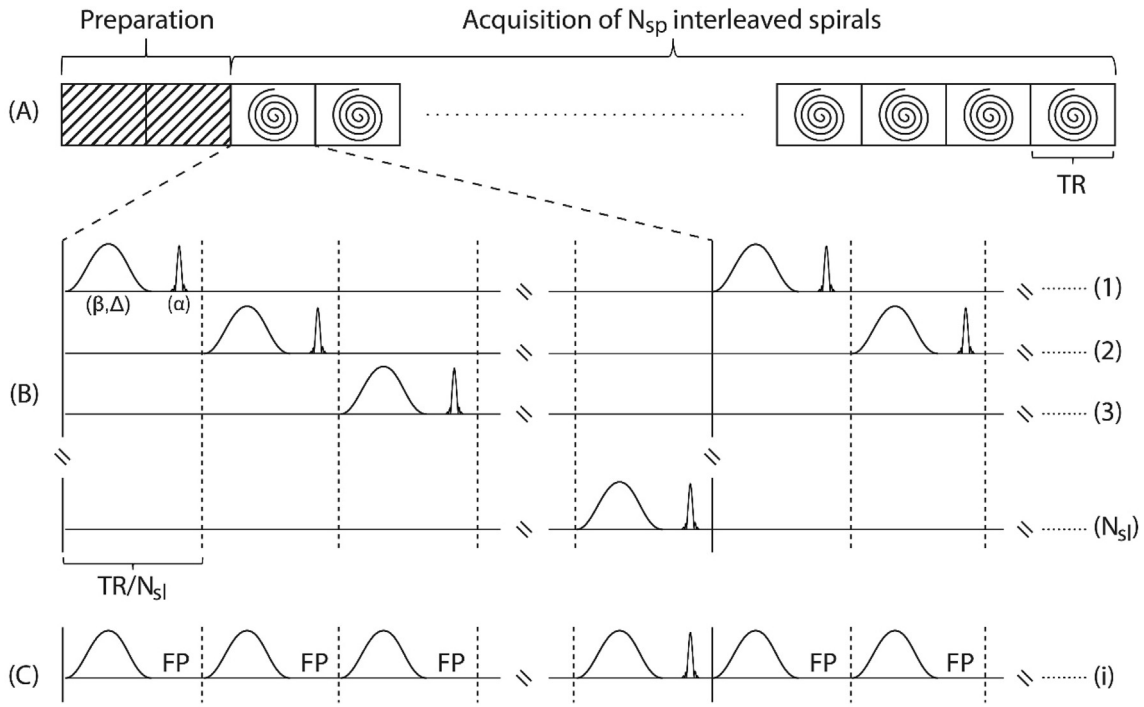

Figure 1. Scheme of the proposed MT-weighted multi-slice interleaved spiral SPGR sequence. (A) After a dummy preparation period of two TR, data in each slice is sampled by N_{sp} spiral interleaves separated by TR. (B) Within each TR, N_{sl} slices are acquired in an interleaved manner. For each slice, MT preparation with a non-selective Gaussian-shaped saturation pulse of variable frequency offset (Δ) and variable flip angle (β) preceded slice excitation with a flip angle (α) using a sinc-shaped excitation pulse. (C) From the interleaved slice acquisition, each slice excitation effectively preceded a train of N_{sl} MT-saturation pulses separated by short free precession (FP) periods.

duration T_{RF} and the shape $\omega_1(t) = \gamma|B_1(t)|$ of the MT pulse.

Consequently, if a fractional saturation of the free pool due to the given train of MT pulses is avoided, the steady state signal S may approximate the situation that is established by a long period of continuous-wave irradiation of the restricted pool protons (see Eq. A5 in ref. [5]):

$$S = c.M_{0,f}\frac{R_{1,r}k_f + R_{1,r}R_{1,f} + R_{1,f}k_r + \bar{W}R_{1,f}}{R_{1,r}R_{1,f} + R_{1,r}k_f + R_{1,f}k_r + \bar{W}R_{1,f} + \bar{W}k_f} \quad (2)$$

where $M_{0,f}$ is the equilibrium magnetization of the free pool; $R_{1,r}$ and $R_{1,f}$ are the longitudinal relaxation rates of the restricted and of the free pool, respectively; k_f and k_r are the first order exchange rates between the free and the bound pool protons, respectively; and c collects all other parameters, such as coil sensitivities. The exact value of R_{1r} has only a minor influence on MT imaging [5]. Following Yarnykh [8], $R_{1,r} = R_{1,obs}$ is chosen, leading to $R_{1,f} = R_{1,obs}$ (cf. Eq. [10] in Ref. [5]). In this work, $R_{1,obs} = R_{1,r} = R_{1,f} = 1/T_1$ is derived from a spiral VFA measurement. Overall, excellent agreement between the spiral VFA method and IR reference measurements were observed [15].

For validation purposes, numerical simulations of the set of coupled Bloch equations including the exchange of longitudinal magnetization in the two-pool model were performed as described in detail, elsewhere [19]. Within the context of this work, however, perfect spoiling of transverse magnetization was assumed (note that an interleaved acquisition scheme with a TR of 1650 ms was used) and it was presumed that the offset frequency of the MT-saturation pulse will be chosen large enough to avoid any direct fractional saturation effects of the free pool. For numerical simulation of the steady state signal, we thus proceeded as follows:

MT-pulses were simulated using the coupled Bloch equations, which are reduced to a set of two coupled differential equations for the longitudinal magnetization components,

$$\frac{dM_{z,f}}{dt} = R_{1,f}\left(M_{0,f} - M_{z,f}\right) - k_f M_{z,f} + k_r M_{z,r} \quad (3a)$$

$$\frac{dM_{z,r}}{dt} = R_{1,r}(M_{0,r} - M_{z,r}) + k_f M_{z,f} + k_r M_{z,r} - \pi\omega_1^2(t)G(\Delta) \quad (3b)$$

Note that the train of MT pulses is interleaved by free-precession periods which were simulated by setting ω_1 in Eq. (3b) equal to zero. At the end of the pulsed-MT-free-precession train, RF excitation of the free pool occurs, which was assumed to act instantaneously on the longitudinal com-

ponent of the free pool. The overall succession of MT-pulses, free precession periods, and RF excitation, was repeated until a steady state was reached; which was typically established after two to three repetitions.

A standard ODE solver was used to simulate the time evolution of the longitudinal magnetization components according to Eq. 3 with common white and gray matter MT tissue parameters [20].

Data evaluation

Whole-brain voxel-wise B_1 maps, together with B_1-corrected $T_{1,B1}$ and B_1-uncorrected T_1 maps were generated from the two VFA spiral SPGR scans as described elsewhere [13], whereas ΔB_0 maps were derived from the phase factor $e^{-i\gamma\Delta B_0(TE_2-TE_1)}$, relating to the two low-resolution SPGR phase images, acquired with different echo times TE_1 and TE_2. Generally, B_1 effects enter the MT model (cf. Eqs. (1) and 2) by: (*i*) a modulation of $\omega_1^2 \mapsto \zeta_{B1}^2 \cdot \omega_1^2$, and (*ii*) a correction of the observed $T_1 \rightarrow T_{1,B1}$; field inhomogeneities lead to a shift of the off-resonance irradiation frequency $\Delta \mapsto \Delta - \Delta B_0$. Finally, voxel-wise estimates for the pool-size ratio F, k_f, and T_{2r} were derived from a non-linear least-squares (NLLS) fit of Eqs. (1) and (2) to a set *S* of MT-weighted signal observations.

The standard software package FSL (FMRIB Software Library v6.0, Oxford, UK) was used for co-registration and skull stripping of the MRI datasets. All other image postprocessing, simulations and visualizations were performed using MATLAB R2019a (The MathWorks, Natick, MA).

In-vivo imaging

Three volunteers were scanned at 3 T (MAGNETOM Prisma, Siemens Healthcare, Erlangen, Germany) using a 20-channel receive head coil. Written informed consent was obtained from participants and measurements were approved by our local ethics committee.

Quite some effort has been undertaken to find optimal sets of MT sampling points that yield robust MT parameter estimates within clinically acceptable scan times [17,21]. For 3D scans, about 10 measurements are required [17,21]. Similarly, Ramani et al. [6] observed a minimum number of about 10 MT measurements using a 2D multi-slice approach with six offset frequencies (Δ) ranging from 1 – 15 kHz

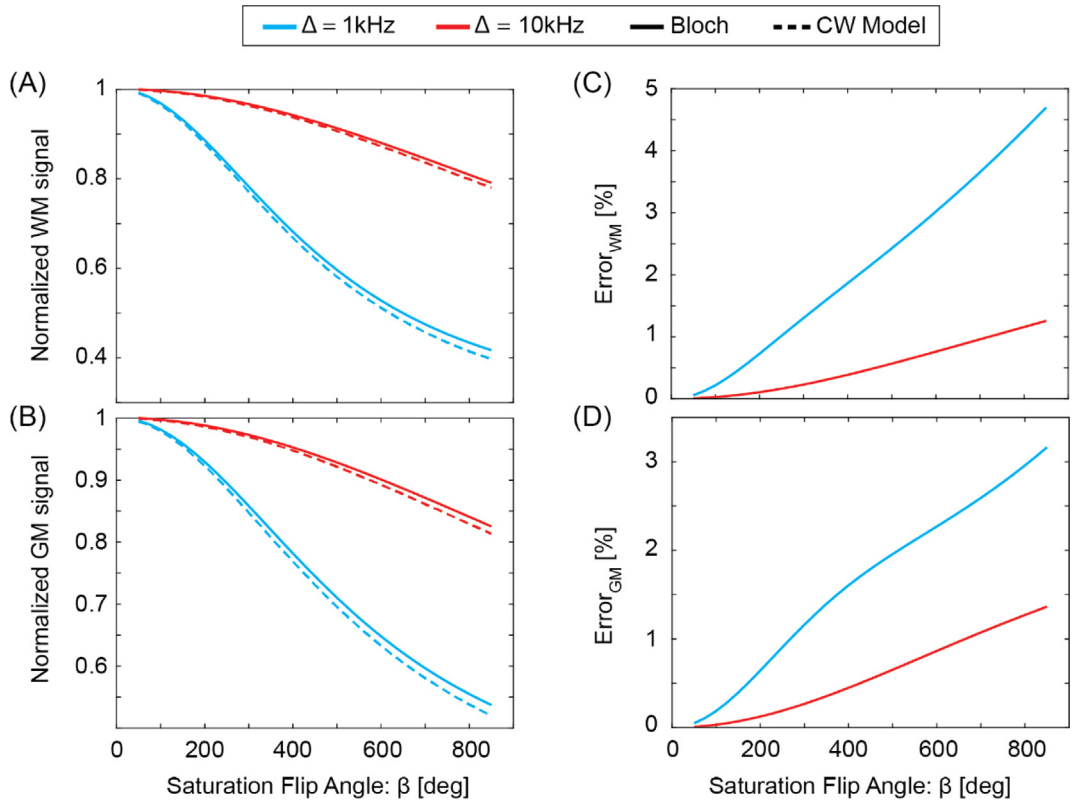

Figure 2. Bloch simulation (solid line) versus CW two-pool model predictions (Eq. (2), dashed line) for typical MT parameter values at 3 T for (A) white matter (F = 13.7 %, $k_f = 4.3\ s^{-1}$, $R_{1,f} = 1.17\ s^{-1}$, $T_{2r} = 12\ \mu s$), (B) gray matter (F = 6.2 %, $k_f = 1.8\ s^{-1}$, $R_{1,f} = 0.8\ s^{-1}$, $T_{2r} = 10\ \mu s$), and their relative difference (C, D) as a function of the saturation flip angle β at two different offset irradiation frequencies.

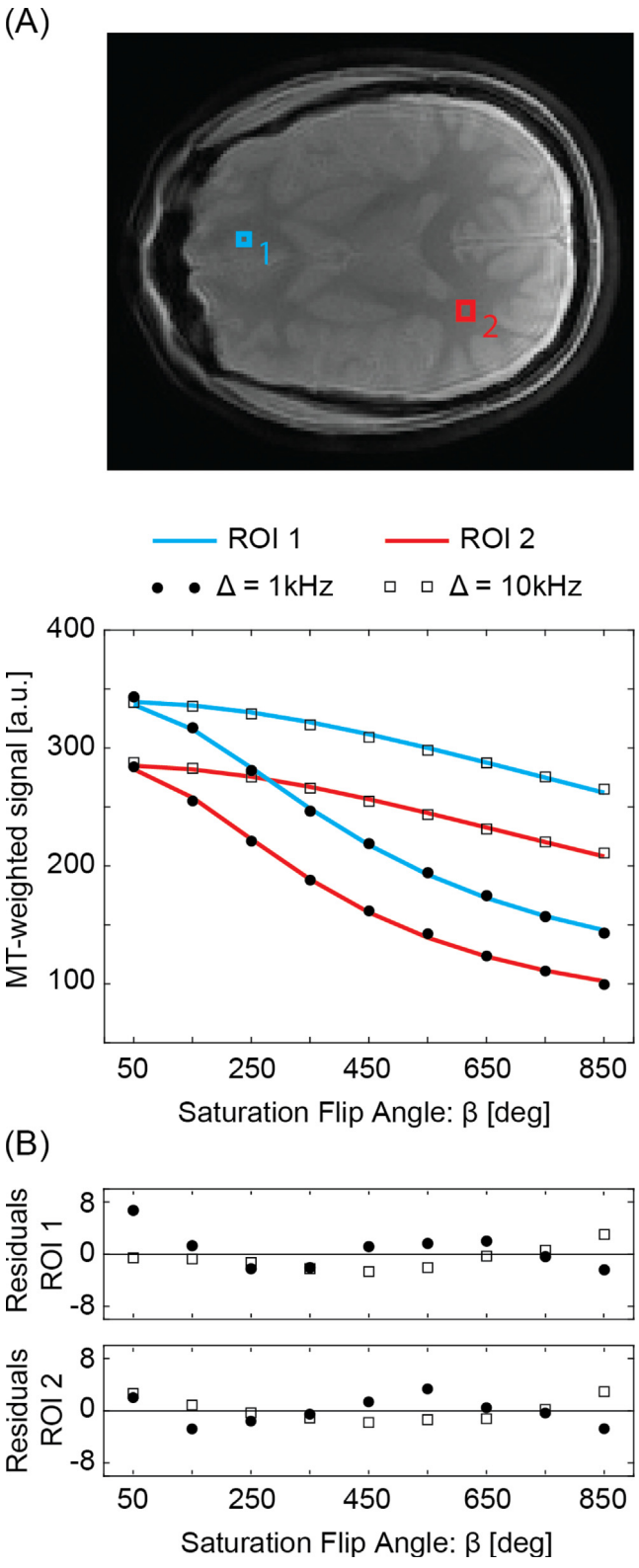

using three different saturation flip angles (β). Furthermore, it was observed that at least one point (potentially better two points) with either large Δ or small β (and thus with no MT weighting) should be included [21].

Following Ramani [6], a lower limit of Δ_{min} = 1 kHz was used to mitigate direct saturation effects (cf. Eq. (2)), whereas the upper bound for the saturation flip angle was β_{max} = 850 deg due to limits from the specific absorption rate (SAR). The upper limit of Δ_{max} = 10 kHz was configured to maximize the MT signal sensitivity to F and T_{2r} [22]. No MT weighting was achieved from using a lower bound of β_{min} = 50 deg. In order to explore a range of 18 down to 6 MT sampling points for subsequent qMT parameter estimation, two base sets of MT-weighted data were acquired:

$$S_1 := \{\Delta = 1, 10\,[\text{kHz}] \wedge \beta = 50, 150, 250, 350, 450, 550, 650, 750, 850\,[\text{deg}]\}$$

$$S_2 := \{\Delta = 1, 10\,[\text{kHz}] \wedge \beta = 50, 184, 316, 450, 584, 716, 850\,[\text{deg}]\}$$

From the base sets, the following subsets were synthesized and also analyzed:

$$S_3 := \{\Delta = 1, 10\,[\text{kHz}] \wedge \beta = 50, 250, 450, 650, 850\,[\text{deg}]\}$$

$$S_4 := \{\Delta = 1, 10\,[\text{kHz}] \wedge \beta = 50, 316, 584, 850\,[\text{deg}]\}$$

$$S_5 := \{\Delta = 1, 10\,[\text{kHz}] \wedge \beta = 50, 450, 850\,[\text{deg}]\}$$

The scan times for the base sets S_1 (2 × 9 scans) and S_2 (2 × 7 scans) were 6:00 min and 4:40 min; respectively. The synthetic data sets S_3 (2 × 5 scans), S_4 (2 × 4 scans) and S_5 (2 × 3 scans) have notional scan times of 3:20 min, 2:40 min and 2:00 min, respectively. For qMT imaging, this leads to scan times that range from 7:15 min down to 3:15 min (including 53 s for the two VFA scans for B_1-T_1-mapping and 22 s for the two GRE scans for ΔB_0 mapping).

Results

Fig. 2 shows a comparison of the continuous-wave (CW) approximation (Eq. (2)) with numerical simulations for white and gray matter using parameter values from [20].

Figure 3. (A) In-vivo CW two-pool model analysis (solid line) of MT-weighted signals from set S_1 for two regions of interest, located in cortical brain tissue (ROI1, blue box, ΔB_0 = 2.9 Hz, ζ_{B1} =1.11) and in the white matter (ROI2, red box, ΔB_0 = 90 Hz, ζ_{B1} = 0.98). Square dots correspond to regional average signals from the MT-weighted images acquired with an offset frequency of Δ = 10 kHz, whereas round dots are representing regional average signals from MT-weighted images acquired with Δ = 1 kHz. (B) Fitting residuals.

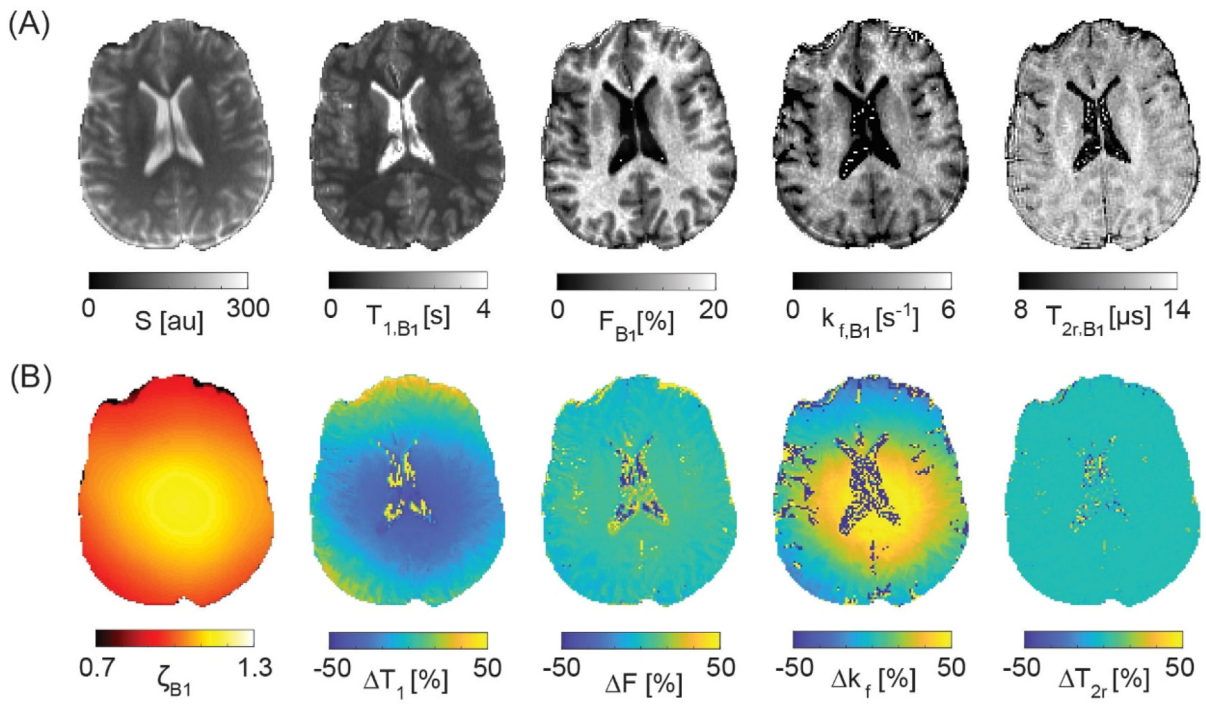

Figure 4. B_1 bias on qMT model parameters. (A) B_1-corrected $T_{1,B1}$, F_{B1}, $k_{f,B1}$, and $T_{2r,B1}$ parameter maps. (B) B_1-map together with its relative contribution to uncorrected T_1, F, k_f, and T_{2r} parameter estimates.

Within the range of experimentally applied offset irradiation frequencies (1 and 10 kHz) and saturation flip angles ($\beta = 50$ to 850 deg) the CW solution overestimates MT-saturation effects by maximal 1.5% at 10 kHz, and at 1 kHz the maximum relative error amounts to less than 5% for WM and less than 3.5% for GM. In summary, good agreement between the CW solution and the numerical simulations was found.

Fig. 3 summarizes in-vivo CW model fitting results (Eqs. (1,2)) for the average signal of two small, presumably homogeneous, regions of interest (ROI1 = 42 pixels, ROI2 = 24 pixels) using data from the 18-samples set S_1. Overall, the fitting residuals indicate appropriate modelling of the data. Upon B_1 and ΔB_0 correction, T_1 and qMT parameter estimates for ROI1 ($\Delta B_0 = 2.9$ Hz, $\zeta_{B1} = 1.11$) change for T_1 from 1182 ms to 873 ms, for F from 14.3 ± 1.2 % to 15.0 ± 1.2 %, for k_f from 3.1 ± 0.4 s^{-1} to 4.2 ± 0.6 s^{-1}, and for T_{2r} from 12.0 ± 0.4 µs to 12.0 ± 0.4 µs. For ROI2 ($\Delta B_0 = 90$ Hz, $\zeta_{B1} = 0.98$), T_1 is changed from 1526 ms to 1597 ms, F is changed from 7.7 ± 0.7 % to 7.4 ± 0.7 %, k_f is changed from 1.9 ± 0.3 s^{-1} to 1.8 ± 0.3 s^{-1}, and T_{2r} is changed from 11.3 ± 0.5 µs to 11.2 ± 0.5 µs. In summary, k_f is most sensitive to and severely affected only by B_1 field miscalibrations, F is affected by both B_1 and ΔB_0 field variations but more strongly by B_1 than ΔB_0 field miscalibrations, whereas the overall bias in T_{2r} appears neglectable.

This finding is further corroborated and summarized in Fig. 4, showing the overall bias as introduced by B_1 field miscalibrations only on both T_1 and qMT parameter maps for a single axial slice using again the data from the 18-samples set S_1. The typical B_1 range of about ±25 % at 3 T results in an about two-fold stronger bias in k_f (±50 %), whereas variations in F are about three-fold less (±8 %). Generally, T_{2r} estimates are not affected by B_1. This is in contrast to ΔB_0 field variations where the maximum observed local off-resonances near the nasal cavity in the order of about +100 Hz lead to local variations in F by a few percent (less than about -3 %) and to overall changes in T_{2r} by less than about 1 %. The forward exchange rate, k_f, is unaffected (see Fig. 5 for the assessment of ΔB_0-field miscalibrations on qMT parameter maps).

Figs. 3, 4 and 5 were derived using the 18-samples set S_1. In Fig. 6, the effect of reduced sample sizes (and thus shortened scan times) on qMT parameter estimation is shown. Generally, qMT parameter maps show no marked fitting failures, even for the 6-samples set S_5. As can be expected, however, the uncertainty in the parameter estimates increases with decreasing number of samples: for a ROI in WM (cf. Fig. 6), F and k_f estimates change from 16.3 ± 1.1 % in set S_1 to 16.2 ± 2.1 % in the 10-samples set S_3 to 15.2 ± 5.2 % for the 6-samples set S_5, and from 3.7 ± 0.4 s^{-1} in S_1 to 3.8 ± 0.8 s^{-1} in S_3 to 4.2 ± 2.6 s^{-1} in

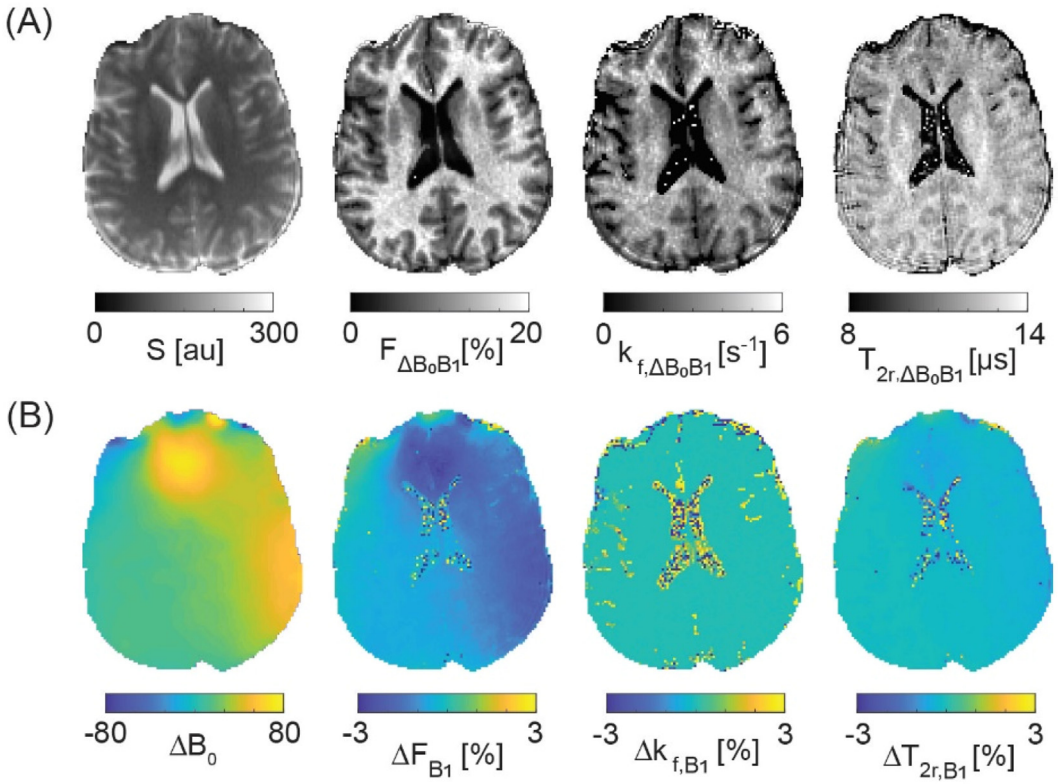

Figure 5. ΔB_0 bias on B_1-corrected qMT model parameters. (A) ΔB_0-B_1-corrected $F_{\Delta B0B1}$, $k_{f,\Delta B0B1}$ and $T_{2r,\Delta B0B1}$ parameter maps. (B) ΔB_0-map together with its relative contribution to B_1-corrected F_{B1}, $k_{f,B1}$ and $T_{2r,B1}$ parameter estimates.

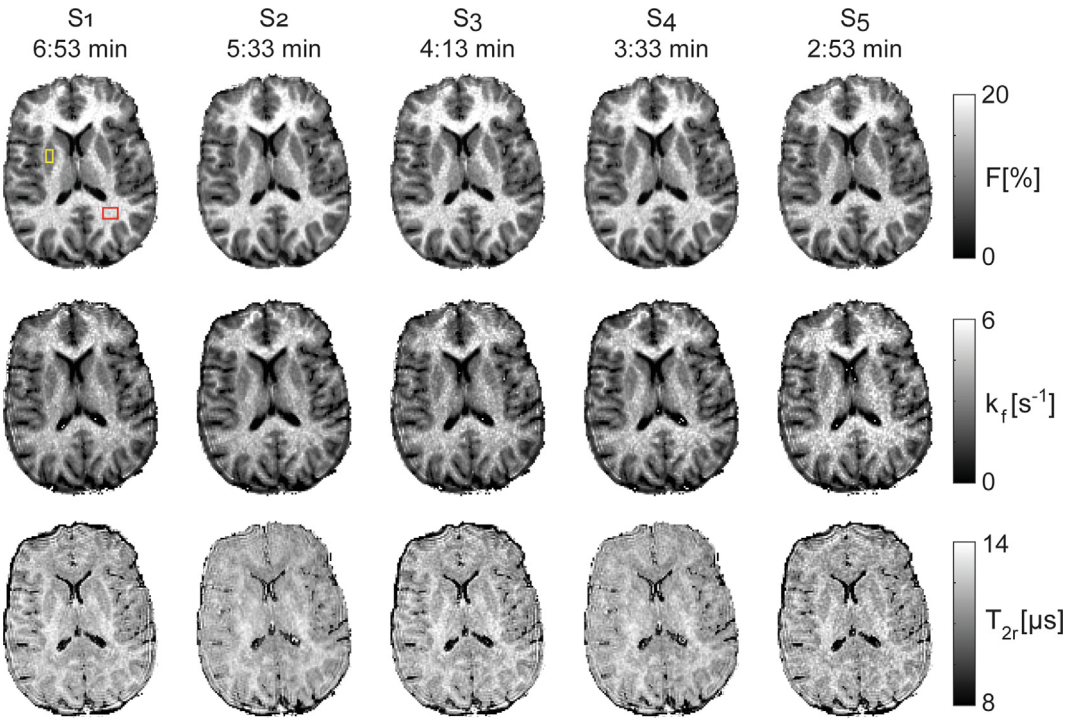

Figure 6. Effect of sampling point reduction on B_1-corrected qMT parameter estimates.

S_5, respectively. Overall, a similar trend is observed for T_{2r} and similar observations were made for gray matter.

Discussion

Generally, qMT parameter mapping requires a set of measurements with different MT-weighting and might thus suffer from over-lengthy scan time requirements in the clinical setting. One obvious strategy to reduce scan time is to reduce the number of MT sampling points and state-of-the-art methods typically require about a minimum of 10 sampling points [17,21]. Alternatively, efficient sequences that offer short repetition times, such as bSSFP, can be used to reduce the overall scan time [10]. Ideally, however, efficient signal acquisition is combined with a low number of sampling points. To this end, in this work, rapid whole-brain qMT imaging was explored using an interleaved multi-slice spiral research sequence at 3 T for combined B_1 and T_1 mapping, as well as for the acquisition of a set of MT-weighted signals with different saturation powers and off-resonances. Due to the interleaved multi-slice acquisition, a simple two-compartment CW MT model could be used to model the data. Without ΔB_0 correction, the total scan time of the investigated B_1-corrected qMT protocols ranges from 6:53 min for the 18-samples set down to 4:13 min for the 10-samples set and finally down to 2:53 min for the 6-samples set, yielding 50 slices with a resolution of $1.3\times1.3\times3.0$ mm^3 for T_1, F, k_f and T_{2r}.

Conventional qMT methods use sampling schemes covering a broad range of off-resonances (Δ) at a rather limited number of MT saturation powers (β) [6,19,23]. In this work, MT contrast was explored using a broad range of saturation powers measured at two off-resonances. The latter approach was preferred since conventional methods include low off-resonances ($\Delta < 1$kHz) but Eq. (2) does not account for direct saturation effects. Thus, MT saturation cannot be explored at low off-resonance frequencies. No such restriction, however, applies for the MT saturation power. Moreover, a different signal model is used, and it is a priori unclear whether conventional optimal sampling schemes apply here as well.

Overall, no systematic investigation was performed to find the optimal $\{\beta,\Delta\}$ sampling pattern for a given number of measurements. Thus, different $\{\beta,\Delta\}$ patterns might be found that even lead to more robust parameter estimates. The 6-point sampling pattern, however, embraces 3 MT saturation powers at two offset frequencies and comes close to the minimal number of scans required [17], indicating a reasonable choice of the sampling pattern. The 10-point sampling scheme together with the combined B_1-T_1 mapping can be performed in less than 5 minutes. Overall, estimated MT parameters were well within the range of what was previously reported [19].

In contrast to related work [24], a higher B_1 bias is observed for F upon using B_1 uncorrected VFA T_1 values (for the settings used here, about three-fold). Consequently, appropriate B_1 correction appears mandatory but requires no extra scan time using the proposed rapid dual-contrast VFA approach [13]. This is in contrast to ΔB_0, where the typical maximum bias on F is limited to a few percent and is negligible for all other qMT parameter estimates. Thus, the bias in F from ΔB_0 is on the order of the uncertainty of the measurement, especially for measurements using 10 or less sampling points. Thus, whether ΔB_0 correction needs to be performed depends on the desired accuracy for the qMT parameter estimates, as well as whether the additional required 22 s needs to be spent or not.

Conclusion

A fast qMT imaging method is proposed based on two variants of an interleaved multi-slice spiral research sequence at 3 T. B_1-correction was mandatory for appropriate MT parameter estimation while the overall effect of ΔB_0 can be neglected. The 10-point MT-weighted sampling scheme together with the B_1-T_1 acquisition offers whole-brain qMT imaging with clinically relevant resolutions in less than 5 minutes and thus offers excellent prospects for widespread clinical translation and use.

Data Availability Statement

The code used to extract the data is distributed by the authors as open-source. The patient data can be made available on request due to privacy/ethical restrictions.

Declaration of Competing Interest

The authors declare the following financial interests/personal relationships which may be considered as potential competing interests: One of the authors, Josef Pfeuffer, is employed by Siemens Healthineers.

Acknowledgements

Swiss National Science Foundation, Grant/Award Number: SNF 325230_182008.

References

[1] Wolff SD, Balaban RS. Magnetization transfer contrast (MTC) and tissue water proton relaxation in vivo. Magn Reson Med 1989;10 (1):135–144. https://doi.org/10.1002/mrm.1910100113.

[2] Dousset V et al.. Experimental allergic encephalomyelitis and multiple sclerosis: lesion characterization with magnetization

transfer imaging. Radiology 1992;182(2):483–491. https://doi.org/10.1148/radiology.182.2.1732968.
[3] Tofts PS et al.. Sources of variation in multi-centre brain MTR histogram studies: body-coil transmission eliminates inter-centre differences. Magn Reson Mater Phy 2006;19(4):209–222. https://doi.org/10.1007/s10334-006-0049-8.
[4] Samsonov A, Alexander AL, Mossahebi P, Wu Y-C, Duncan ID, Field AS. Quantitative MR imaging of two-pool magnetization transfer model parameters in myelin mutant shaking pup. Neuroimage 2012;62(3):1390–1398. https://doi.org/10.1016/j.neuroimage.2012.05.077.
[5] Sled JG, Pike GB. Quantitative interpretation of magnetization transfer in spoiled gradient echo MRI sequences. J Magn Reson 2000;145(1):24–36. https://doi.org/10.1006/jmre.2000.2059.
[6] Ramani A, Dalton C, Miller DH, Tofts PS, Barker GJ. Precise estimate of fundamental in-vivo MT parameters in human brain in clinically feasible times. Magn Reson Imaging 2002;20(10):721–731. https://doi.org/10.1016/S0730-725X(02)00598-2.
[7] Henkelman RM, Huang X, Xiang QS, Stanisz GJ, Swanson SD, Bronskill MJ. Quantitative interpretation of magnetization transfer. Magn Reson Med 1993;29(6):759–766. https://doi.org/10.1002/mrm.1910290607.
[8] Yarnykh VL. Fast macromolecular proton fraction mapping from a single off-resonance magnetization transfer measurement. Magn Reson Med 2012;68(1):166–178. https://doi.org/10.1002/mrm.23224.
[9] Yarnykh VL. Time-efficient, high-resolution, whole brain three-dimensional macromolecular proton fraction mapping. Magn Reson Med 2016;75(5):2100–2106. https://doi.org/10.1002/mrm.25811.
[10] Bieri O, Scheffler K. Optimized balanced steady-state free precession magnetization transfer imaging. Magn Reson Med 2007;58(3):511–518. https://doi.org/10.1002/mrm.21326.
[11] Battiston M et al.. Fast bound pool fraction mapping via steady-state magnetization transfer saturation using single-shot EPI. Magn Reson Med 2019;82(3):1025–1040. https://doi.org/10.1002/mrm.27792.
[12] Afshari R, Santini F, Heule R, Meyer CH, Pfeuffer J, Bieri O. One-minute whole-brain magnetization transfer ratio imaging with intrinsic B1-correction. Magn Reson Med 2021;85(5):2686–2695. https://doi.org/10.1002/mrm.28618.
[13] Heule R, Pfeuffer J, Meyer CH, Bieri O. Simultaneous B1 and T1 mapping using spiral multislice variable flip angle acquisitions for whole-brain coverage in less than one minute. Magn Reson Med 2019;81(3):1876–1889. https://doi.org/10.1002/mrm.27544.
[14] Heule R, Bieri O. Rapid and robust variable flip angle T1 mapping using interleaved two-dimensional multislice spoiled gradient echo imaging. Magn Reson Med 2017;77(4):1606–1611. https://doi.org/10.1002/mrm.26246.
[15] Heule R, Pfeuffer J, Bieri O. Snapshot whole-brain T1 relaxometry using steady-state prepared spiral multislice variable flip angle imaging. Magn Reson Med 2018;79(2):856–866. https://doi.org/10.1002/mrm.26746.
[16] Lustig M, Pauly JM. SPIRiT: Iterative self-consistent parallel imaging reconstruction from arbitrary k-space. Magn Reson Med 2010;64(2):457–471. https://doi.org/10.1002/mrm.22428.
[17] Levesque IR, Sled JG, Pike GB. Iterative optimization method for design of quantitative magnetization transfer imaging experiments. Magn Reson Med 2011;66(3):635–643. https://doi.org/10.1002/mrm.23071.
[18] Graham SJ, Henkelman RM. Understanding pulsed magnetization transfer. J Magn Reson Imaging 1997;7(5):903–912. https://doi.org/10.1002/jmri.1880070520.
[19] Sled JG, Pike GB. Quantitative imaging of magnetization transfer exchange and relaxation properties in vivo using MRI. Magn Reson Med 2001;46(5):923–931. https://doi.org/10.1002/mrm.1278.
[20] Sled JG et al.. Regional variations in normal brain shown by quantitative magnetization transfer imaging. Mag Reson Med 2004;51(2):299–303. https://doi.org/10.1002/mrm.10701.
[21] Cercignani M, Alexander DC. Optimal acquisition schemes for in vivo quantitative magnetization transfer MRI. Magn Reson Med 2006;56(4):803–810. https://doi.org/10.1002/mrm.21003.
[22] Boudreau M, Pike GB. Sensitivity regularization of the Cramér-Rao lower bound to minimize B1 nonuniformity effects in quantitative magnetization transfer imaging. Magn Reson Med 2018;80(6):2560–2572. https://doi.org/10.1002/mrm.27337.
[23] Yarnykh VL. Pulsed Z-spectroscopic imaging of cross-relaxation parameters in tissues for human MRI: Theory and clinical applications. Magn Reson Med 2002;47(5):929–939. https://doi.org/10.1002/mrm.10120.
[24] Boudreau M, Stikov N, Pike GB. B1-sensitivity analysis of quantitative magnetization transfer imaging. Magn Reson Med 2018;79(1):276–285. https://doi.org/10.1002/mrm.26673.

Please cite this article as: R. Afshari, F. Santini, R. Heule et al., Rapid whole-brain quantitative MT imaging, Z Med Phys, https://doi.org/10.1016/j.zemedi.2023.02.005